

**Supplemental material**

**Accelerate gas diffusion-weighted MRI for lung morphometry with deep learning**

## Network architecture

The deep cascade of residual dense network (DC-RDN) cascades 5 residual dense blocks (RDBs) and 5 data consistency (DC) layers (see Fig. 1). Each RDB consists of 3 components, viz., a feature extraction layer, a dense block, and a reconstruction layer with skip connection. Specifically, the  $d$ -th RDB takes the zero-filling image (when  $d = 1$ ), or the output from the previous DC layer as input (when  $d > 1$ ), denoted as  $\mathbf{x}_{d-1}$ , and subsequently outputs a reconstruction, denoted as  $\mathbf{x}_{d,r}$ .

In the feature extraction layer, feature maps  $\mathbf{M}_{d,f}$  are extracted from the concatenated multiple  $b$ -value DW images  $\mathbf{x}_{d-1}$  ( $\mathbf{x}_0$  denotes the zero-filling image) using a convolution layers with  $3 \times 3$  kernel size and 64 filters followed by batch normalization (BN) and rectified linear unit (ReLU) activation (denoted as  $\sigma$ ). The  $\mathbf{M}_{d,f}$  can be expressed as,

$$\mathbf{M}_{d,f} = \sigma\left(\text{BN}\left(\mathbf{W}_{d,f} * \mathbf{x}_{d-1} + \mathbf{b}_{d,f}\right)\right) \quad (1)$$

where  $\mathbf{W}_{d,f}$  and  $\mathbf{b}_{d,f}$  denote the weight and bias matrices of the feature extraction layer, and  $*$  denotes the convolution operator.  $\mathbf{M}_{d,f}$  is then fed into the following dense block.

The dense block consists of 4 convolution layers with  $3 \times 3$  kernel size and 64 filters, and each convolution layer is also followed by BN and ReLU activation. In the dense block of the  $d$ -th RDB, the  $l$ -th layer receives the feature maps of all preceding layers as input. Therefore, the output of the  $l$ -th layer of the dense block is,

$$\mathbf{M}_{d,l} = \sigma\left(\text{BN}\left(\mathbf{W}_{d,l} * \left[\mathbf{M}_{d,f}, \mathbf{M}_{d,1}, \dots, \mathbf{M}_{d,l-1}\right] + \mathbf{b}_{d,l}\right)\right) \quad (2)$$

where  $\mathbf{W}_{d,l}$  and  $\mathbf{b}_{d,l}$  denote the weight and bias matrices of the  $l$ -th layer of the dense block.

$[\mathbf{M}_{d,f}, \mathbf{M}_{d,1}, \dots, \mathbf{M}_{d,l-1}]$  refers to the concatenation of the feature maps from the feature extraction layer and the convolution layers 1,  $\dots$ ,  $l - 1$  in the dense block, resulting in  $l \times 64$  feature maps.

After the dense block, the reconstruction layer uses a  $1 \times 1$  convolution to fuse the whole feature maps in the  $d$ -th RDB into the residual reconstruction, which can be formulated as,

$$\mathbf{M}_{d,r} = \mathbf{W}_{d,r} * [\mathbf{M}_{d,f}, \mathbf{M}_{d,1}, \dots, \mathbf{M}_{d,4}] + \mathbf{b}_{d,r} \quad (3)$$

where  $\mathbf{W}_{d,r}$  and  $\mathbf{b}_{d,r}$  denote the weight and bias matrices of the reconstruction layer. Through the skip connection, the output of the  $d$ -th RDB is,

$$\mathbf{x}_{d,r} = \mathbf{x}_{d-1} + \mathbf{M}_{d,r} \quad (4)$$

Since the output  $\mathbf{x}_{d,r}$  may not be consistent with the sampled k-space  $\mathbf{y}$ , a DC layer is used to correct the difference between  $\mathbf{x}_{d,r}$  and  $\mathbf{y}$  in k-space domain. Let  $\mathbf{k}_0 = \mathbf{F}\mathbf{x}_0$  and  $\mathbf{k}_{d,r} = \mathbf{F}\mathbf{x}_{d,r}$ , where  $\mathbf{F}$  is the Fourier transform, the corrected k-space  $\mathbf{k}_d$  can be defined as,

$$\mathbf{k}_d(z) = \begin{cases} \mathbf{k}_0(z) & \text{if } z \in \Omega \\ \mathbf{k}_{d,r}(z) & \text{if } z \notin \Omega \end{cases} \quad (5)$$

where  $z$  is the k-space index, and  $\Omega$  is the subset of indices sampled in k-space. The output of the DC layer,  $\mathbf{x}_d$ , is obtained through inverse Fourier transform of  $\mathbf{k}_d$ . Similarly,  $\mathbf{x}_d$  is then adopted as the input of the  $(d + 1)$ -th RDB. Finally, the last DC layer output the reconstruction of the DC-RDN.

### Training data simulation

If hyperpolarized gas ventilation images are considered as the signal without diffusion-sensitizing gradients (donated as  $S_0$ ), the signal of non-zero  $b$ -value (donated as  $S(b)$ ) can be described using the cylinder model [1],

$$S(b) = S_0 \exp(-bD_T) \left[ \frac{\pi}{4b(D_L - D_T)} \right]^{1/2} \cdot \Phi \left[ (b(D_L - D_T))^{1/2} \right] \quad (6)$$

where  $D_L = D_0 F_L \left( bD_0, \frac{r}{R}, \frac{R}{\sqrt{2D_0\Delta}} \right)$ ,  $D_T = D_0 F_T \left( bD_0, \frac{r}{R}, \frac{R}{\sqrt{2D_0\Delta}} \right)$

where  $D_L$  and  $D_T$  are longitudinal and transverse diffusion coefficients,  $\Phi$  is the error function,  $D_0$  is the free diffusion coefficients of  $^{129}\text{Xe}$  in a gas mixture ( $0.14 \text{ cm}^2/\text{s}$ ),  $R$  is acinar duct radius,  $r$  is acinar lumen radius, and  $\Delta$  is the diffusion time, respectively. The phenomenological expressions of  $F_L$  and  $F_T$  have been derived by Sukstanskii et al [1].

The parameters  $R$  and  $r$  were sampled uniformly from the general distribution of lung microscopic dimensions of the acinar airways:  $R \in (360 \pm 60) \mu\text{m}$ ,  $r \in (160 \pm 30) \mu\text{m}$  [1]. Other parameters were the same as those used in the testing data acquisition:  $\Delta = 5 \text{ ms}$ ,  $b = 0, 10, 20, 30, 40 \text{ s/cm}^2$ . Then the synthetic multiple  $b$ -value DW-MRI data could be produced using Equation 6, which served as the reference in the training process. In order to avoid overfitting and improve the generalization performance of DC-RDN, data augmentations including rotations ( $90^\circ$ ,  $180^\circ$ , and  $270^\circ$ ) and horizontal flip were applied on each synthetic DW image.

## Evaluation

Additionally, qualitative image quality was evaluated in an independently and blinded fashion by two experienced readers using a 4-point ordinal scale [2,3], including sharpness (1, no blurring; 2, mild blurring; 3, moderate blurring; 4, severe blurring), signal-to-noise ratio (SNR) (1, excellent; 2, good; 3, fair; 4, poor), aliasing artifacts (1, none; 2, mild; 3, moderate; 4, severe), and overall image quality (1, excellent; 2, good; 3, fair; 4, poor). Scoring evaluations were performed for each slice based on the  $b = 0$  image.

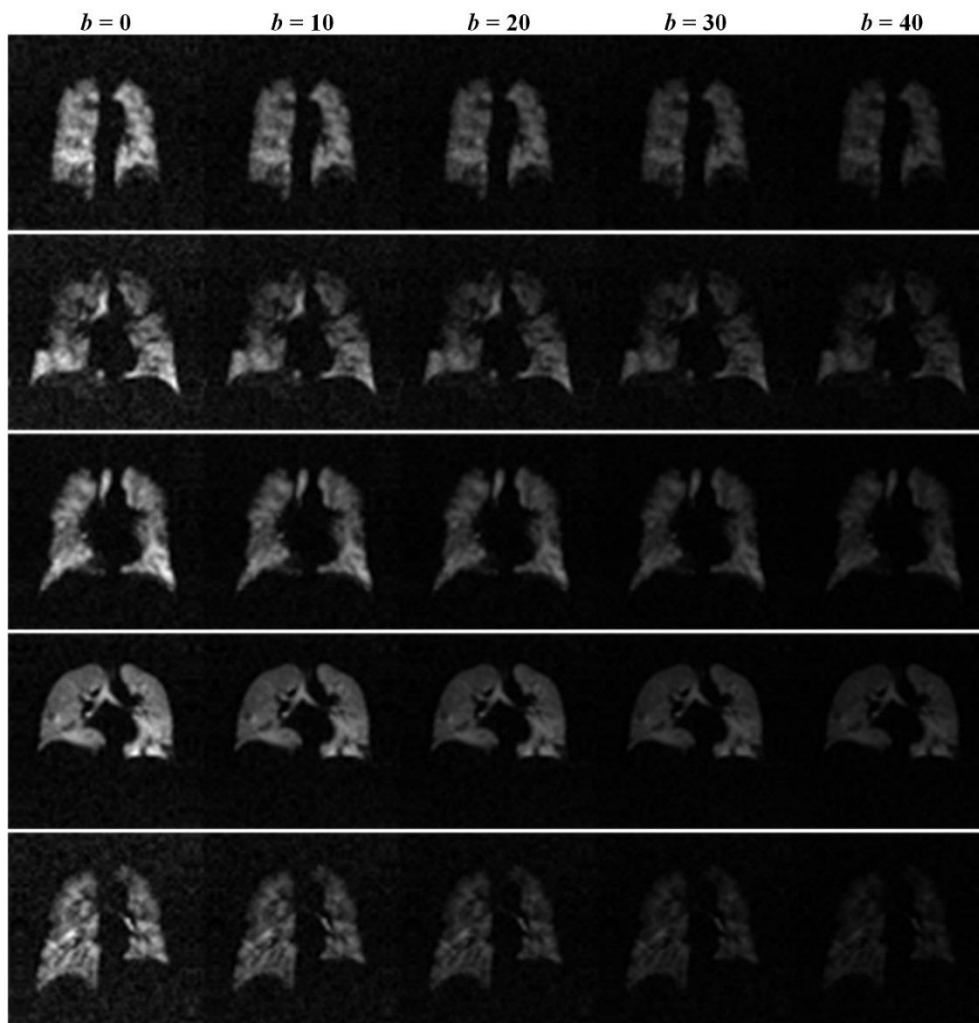
## References

1. Sukstanskii AL, Yablonskiy DA (2012) Lung morphometry with hyperpolarized  $^{129}\text{Xe}$ :

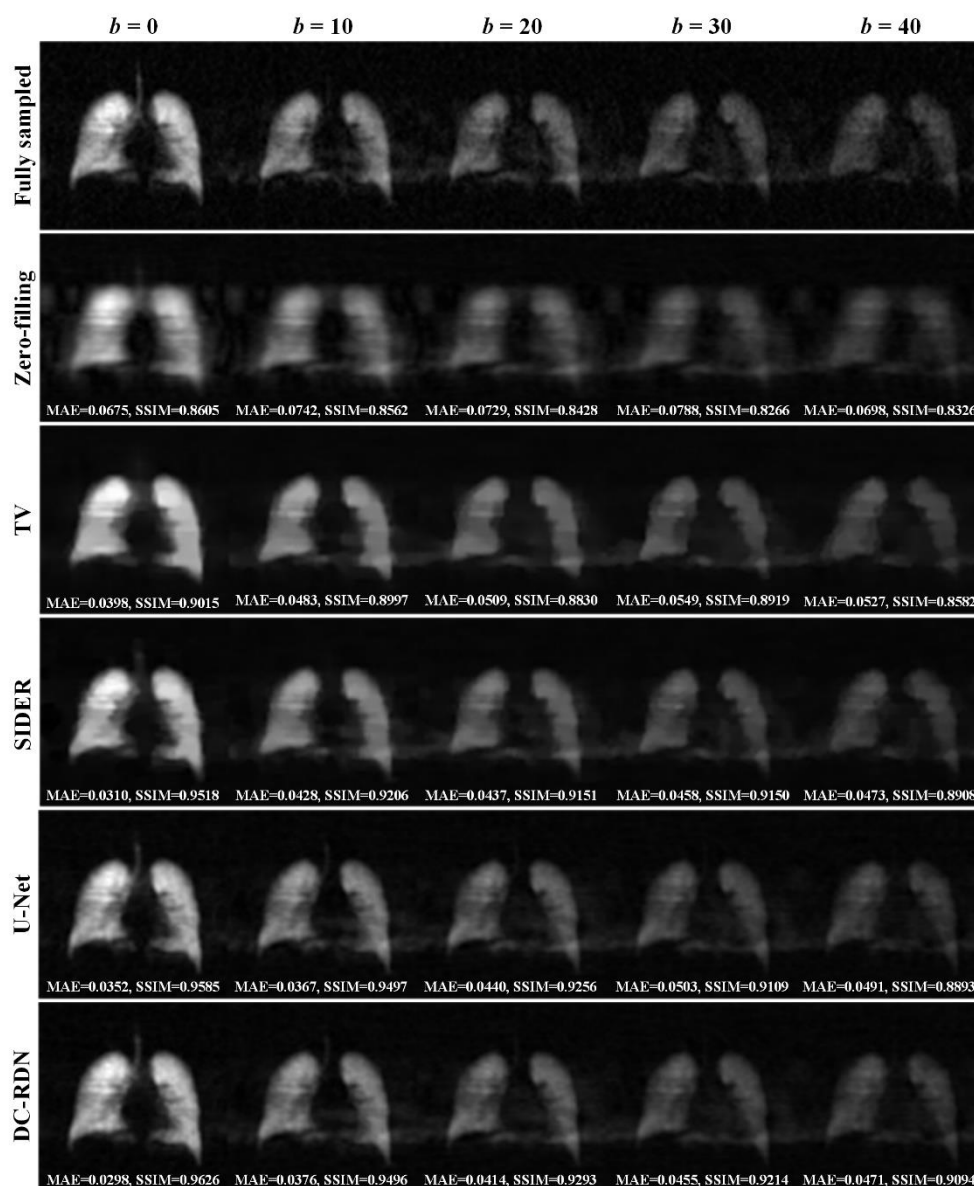
theoretical background. *Magn Reson Med* 67:856-866.

2. Hammernik K, Klatzer T, Kobler E, et al (2018) Learning a variational network for reconstruction of accelerated MRI data. *Magn Reson Med* 79:3055-3071.
3. Yaman B, Hosseini SAH, Moeller S, et al (2020) Self-supervised learning of physics-guided reconstruction neural networks without fully sampled reference data. *Magn Reson Med* 84:3172-3191.

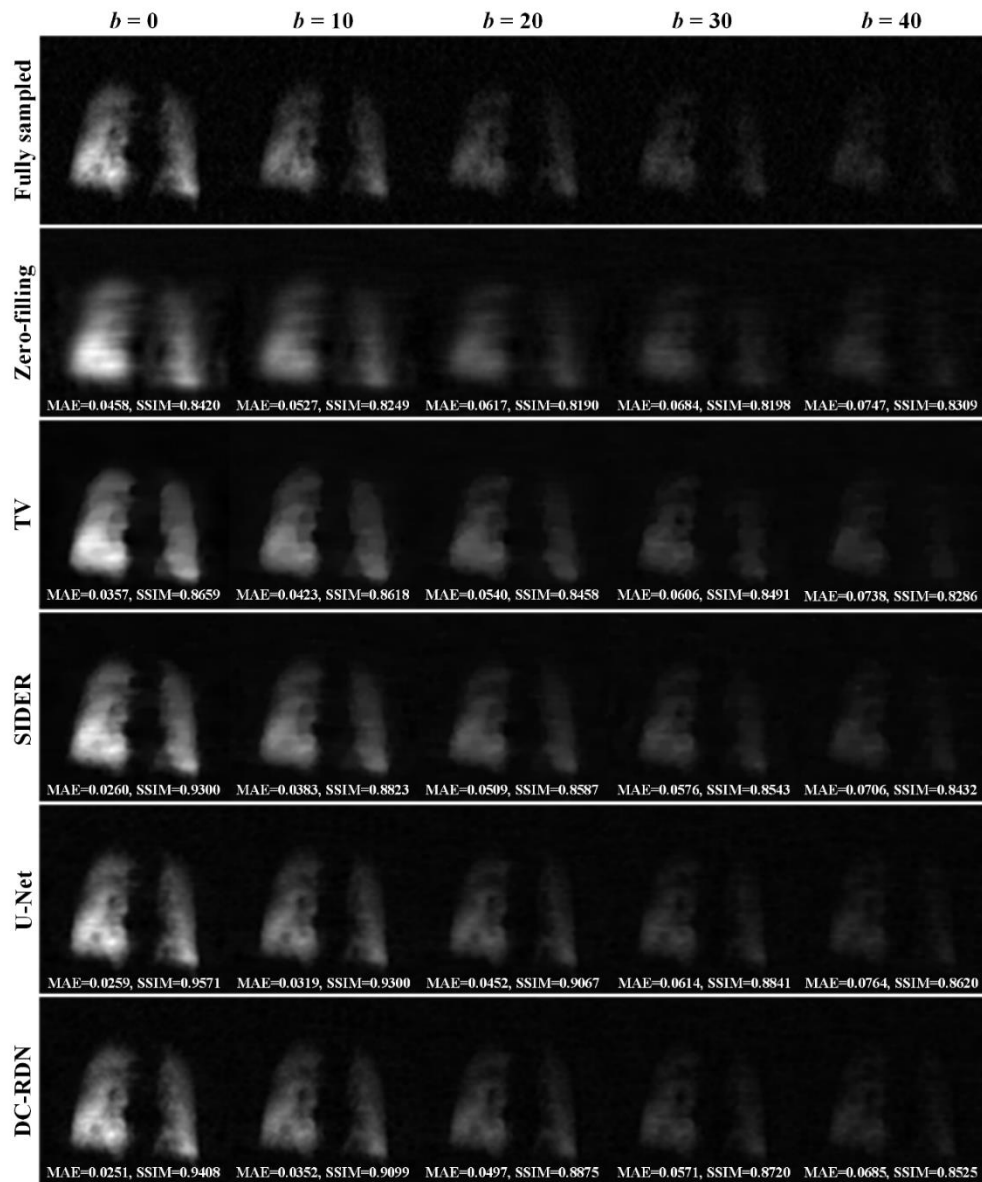
**Supplementary Fig. 1** Examples of synthetic multiple  $b$ -value  $^{129}\text{Xe}$  DW images. Compared with real multiple  $b$ -value gas DW-MRI data, a similar decrease of signal intensity with an increasing  $b$ -value is observed in the synthetic DW images. This indicates the effectiveness of the simulation strategy used in this work. DW, diffusion-weighted



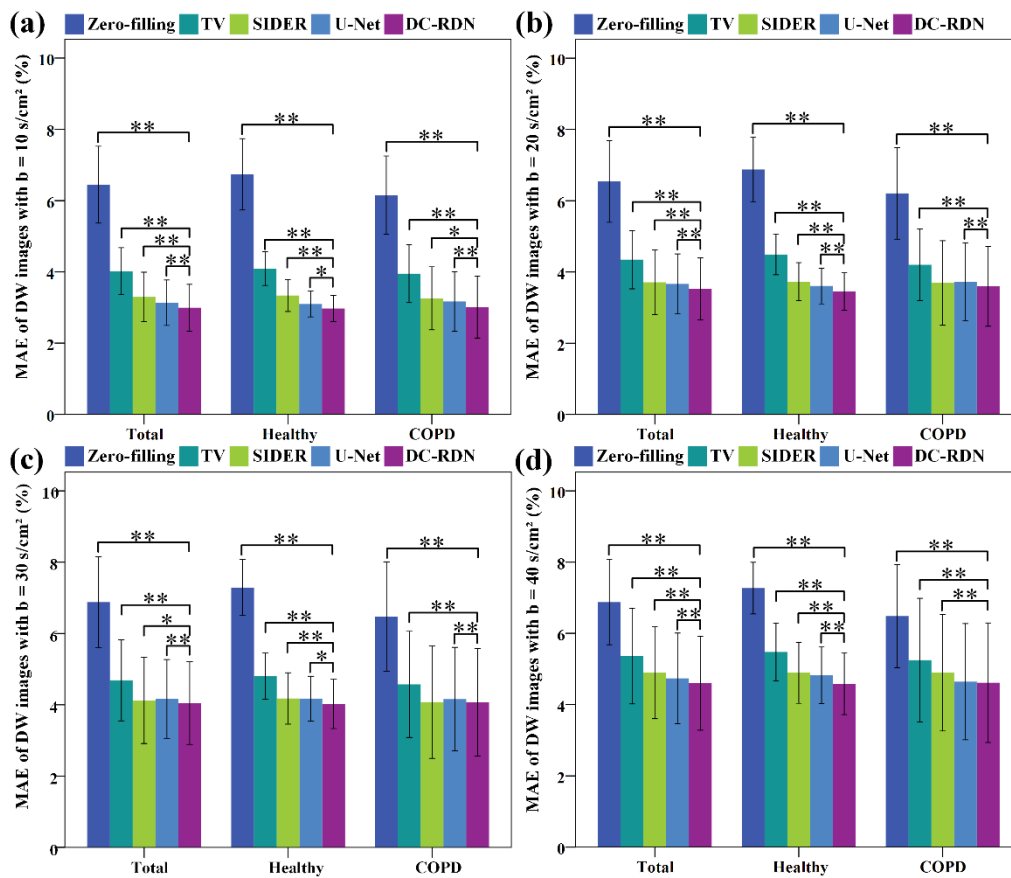
**Supplementary Fig. 2** The corresponding reconstructed results with  $b = 0, 10, 20, 30, 40$  s/cm<sup>2</sup> of Fig. 2a1 obtained using the FS, zero-filling, TV, SIDER, U-Net, and DC-RDN, respectively. The quantitative metrics are listed under the images. For all  $b$ -value images, DC-RDN achieves better-preserved lung structures and better quantitative metrics compared with the baseline methods. DC-RDN, deep cascade of residual dense network; FS, fully sampled; MAE, mean absolute error; SIDER, signal decay into the reconstruction; SSIM, structure similarity; TV, total variation



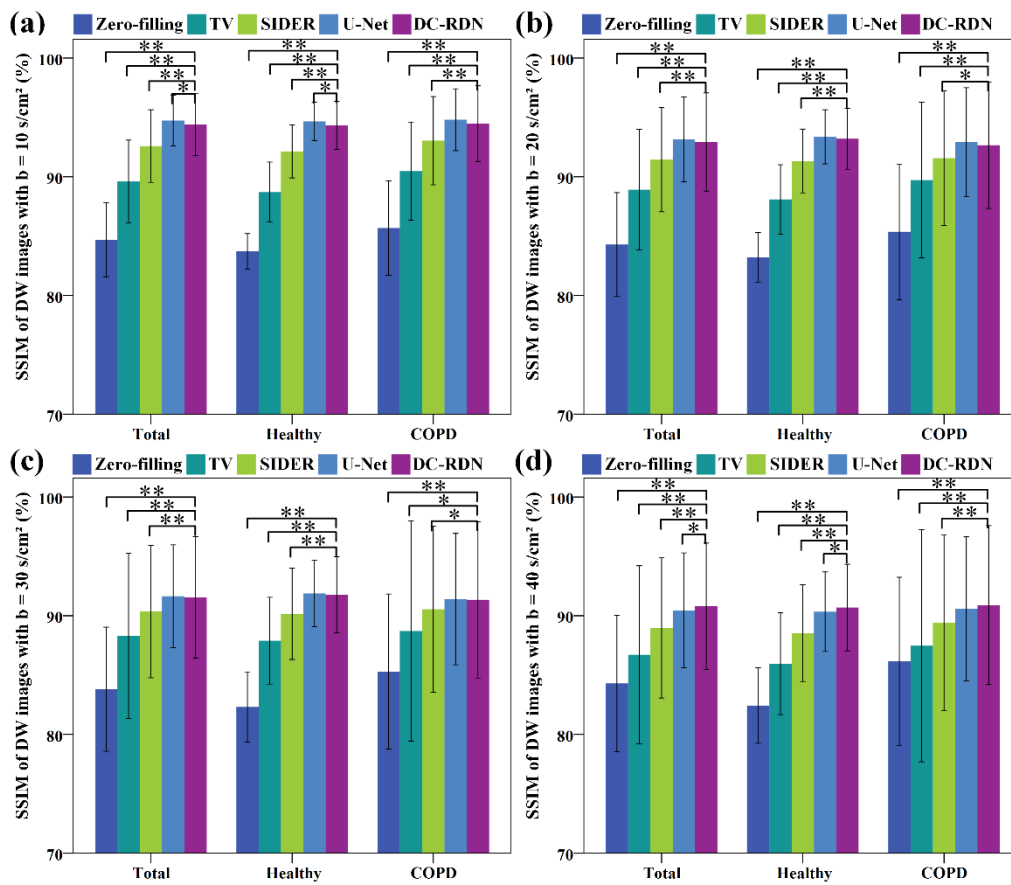
**Supplementary Fig. 3** The corresponding reconstructed results with  $b = 0, 10, 20, 30, 40$  s/cm<sup>2</sup> of Fig. 2a2 obtained using the FS, zero-filling, TV, SIDER, U-Net, and DC-RDN, respectively. The quantitative metrics are listed under the images. DC-RDN provides better depiction of lung structures and restores more details than the baseline methods



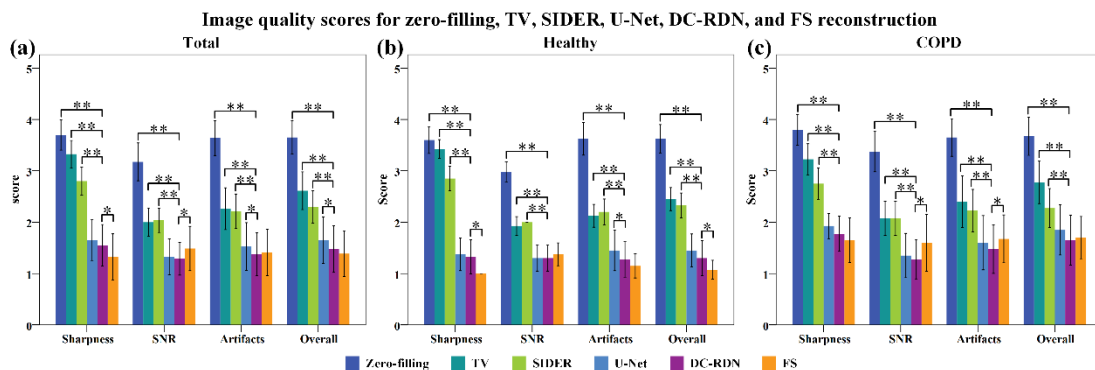
**Supplementary Fig. 4** Average MAE of DW images with  $b$ -values of 10, 20, 30, 40  $s/cm^2$  obtained using the zero-filling, TV, SIDER, U-Net and DC-RDN for the total, healthy and COPD test datasets. \* denotes  $p < 0.05$ , and \*\* denotes  $p < 0.001$ . DC-RDN achieves the lowest MAE values for the nonzero  $b$ -value images compared to the baseline methods. COPD, chronic obstructive lung disease



**Supplementary Fig. 5** Average SSIM of DW images with  $b$ -values of 10, 20, 30, 40  $s/cm^2$  obtained using the zero-filling, TV, SIDER, U-Net and DC-RDN for the total, healthy and COPD test datasets. \* denotes  $p < 0.05$ , and \*\* denotes  $p < 0.001$ . DC-RDN achieves the highest SSIM values for the nonzero  $b$ -value images compared to the two CS-MRI methods, and similar SSIM values compared to the U-Net



**Supplementary Fig. 6** Quantitative comparisons of image quality scores between different reconstruction methods at an acceleration factor of 4. Image quality scores were evaluated independently by two blinded readers in terms of sharpness, SNR, aliasing artifacts, and overall image quality. a-c Average image quality scores values of  $b = 0$  DW images obtained using the zero-filling, TV, SIDER, U-Net, DC-RDN, and FS methods for the total, healthy, and COPD test datasets, respectively. Bar plots show average reader scores and their standard deviation across the test data. \* denotes  $p < 0.05$ , and \*\* denotes  $p < 0.001$ . For all the test data, both the U-Net and DC-RDN approaches get comparable scores to the reference images in terms of sharpness, SNR, aliasing artifacts, and overall image quality. In addition, DC-RDN achieves significantly better image quality than the two CS-MRI methods in terms of all the scoring criteria. SNR, signal-to-noise ratio



**Supplementary Fig. 7** ADC maps estimated from the reconstructed images through different algorithms in a 26-year-old healthy male volunteer and a 53-year-old COPD male patient. a1-f1, a2-f2, ADC maps derived from the FS images and reconstructed results through the zero-filling, TV, SIDER, U-Net and DC-RDN, respectively. The  $MAE_{ADC}$  and slice ADC values are listed under each image. ADC, apparent diffusion coefficient

